

Misaligned gas acquisition as a formation pathway of S0 galaxies

YUREN ZHOU , ^{1, 2, 3} YANMEI CHEN , ^{1, 2, 3} YONG SHI , ^{1, 2, 3} QIUSHENG GU , ^{1, 2, 3} JUNFENG WANG , ⁴ AND DMITRY BIZYAEV , ^{5, 6}

¹*School of Astronomy and Space Science, Nanjing University, Nanjing 210023, China*

²*Key Laboratory of Modern Astronomy and Astrophysics (Nanjing University), Ministry of Education, Nanjing 210023, China*

³*Collaborative Innovation Center of Modern Astronomy and Space Exploration, Nanjing 210023, China*

⁴*Department of Astronomy and Institute of Theoretical Physics and Astrophysics, Xiamen University, Xiamen, Fujian 361005, China*

⁵*Apache Point Observatory and New Mexico State University, PO Box 59, Sunspot, NM 88349-0059, USA*

⁶*Sternberg Astronomical Institute, Moscow State University, Moscow 119992, Russia*

ABSTRACT

We analyze a sample of 753 S0 galaxies from the MPL-10 of MaNGA survey and investigate the gas-star kinematic misalignment and merger remnant fraction in galaxies with different morphological types. The misalign fraction in S0s is the highest among all the morphological types for both young (global $D_n4000 < 1.6$, $\sim 15\%$) and old (global $D_n4000 > 1.6$, $\sim 10\%$) galaxies. We compare the properties of misaligned S0s with other types of galaxies, finding: (i) misaligned S0s and misaligned spirals have higher bulge luminosity, higher B/T and larger Sérsic index compared to spirals; (ii) the misaligned S0s have lower bulge luminosity M_r and smaller bulge size than merger remnant S0s, while aligned S0s have the widest coverage for these parameter distributions which are overlapped with both misaligned S0s and merger remnant S0s; (iii) misaligned S0s have lower stellar mass M_* and more isolated environment than aligned S0s and merger remnant S0s; (iv) the young misaligned S0s have positive D_n4000 radial gradient, while the aligned S0s and merger remnant S0s show negative D_n4000 radial gradient. Combining all these observational results, we suggest misaligned gas acquisition as another efficient formation pathway for S0 galaxies. The redistribution of gas angular momentum during gas-gas collision between accreted and pre-existing gas leads to gas inflow and the growth of bulge component, meanwhile the lack of cold gas at the outskirts leads to fading of spiral arms.

Keywords: galaxies: formation – galaxies: kinematics and dynamics – galaxies: elliptical and lenticular, cD

1. INTRODUCTION

In the theory of galaxy formation and evolution, the morphology of galaxy provides the first clue to their evolutionary status. It is suggested that disks of galaxies are formed by cooling of gas in the dark matter halos (Blumenthal et al. 1984; Mo et al. 1998), while the bulges of galaxies are formed from mergers (Khochfar & Silk 2006). S0 galaxies, which are characterized by featureless disks and clear bulge components (Hubble 1926), remain the subject of numerous debates regarding their formation pathways.

Corresponding author: Yanmei Chen
 chenym@nju.edu.cn

Two formation pathways have been proposed for S0 galaxies. The first one is fading of spiral galaxies (Gunn & Gott 1972; Larson et al. 1980; Quilis et al. 2000). Observations show that the fraction of S0s in the local universe ($z \lesssim 0.06$) increases with their projected local galaxy number density (Dressler 1980, morphology-density relation), which suggests that the environmental processes, like starvation (Larson et al. 1980) or ram-pressure stripping (Gunn & Gott 1972; Quilis et al. 2000), reduce the gaseous content in spiral galaxies and lead to the formation of S0s. The second one includes mergers and galaxy interactions (Icke 1985; Bekki 1998; Bekki & Couch 2011; Querejeta et al. 2015). The S0s are at least luminous in K -band as spiral galaxies (Burstein et al. 2005) and display systematically higher bulge-to-disk ratio (Dressler 1980). These evidences indicate that

mechanisms leading to mass inflow and growth of bulge, such as mergers (Bekki 1998; Querejeta et al. 2015) or galaxy interactions (Icke 1985; Bekki & Couch 2011), play a role in the formation of S0s. However, neither pathway alone can explain all the properties of S0s. On the one hand, Laurikainen et al. (2010) find that the bulges of S0s exhibit properties more similar to spiral galaxies than elliptical galaxies in the M_K^0 - r_{eff} diagram (K -band absolute magnitude M_K^0 and effective radius r_{eff} of bulge) and in the photometric plane (relation between Sérsic index n , r_{eff} and the central surface brightness of the bulge), indicating that mergers are not able to explain the statistical behaviour of bulges. On the other hand, Wilman et al. (2009) discover that S0s are as common in groups as in clusters at intermediate redshift ($z \sim 0.4$) and tend to reside in the outskirts of groups. They propose processes like mergers, galaxy harassment and tidal interactions, which are effective at these locations, should be the most possible mechanisms for the formation of S0s.

Using a sample of S0s from the SAMI Galaxy Survey, Deeley et al. (2020) suggest rotationally supported S0s with v/σ above 0.5 form from faded spirals while pressure-supported S0s with v/σ below 0.5 form from mergers. Based on a sample of nearby S0s with single fiber spectra for the central regions from the Sloan Digital Sky Survey (SDSS) Data Release 7, Xiao et al. (2016) find that star-forming (SF) S0s have the lowest stellar masses compared to other S0s and tend to locate in the low density environment. K. Xu et al. (2022) use a spatially resolved galaxies sample from the Mapping Nearby Galaxies at Apache Point Observatory (MaNGA) survey to show that SF S0s have bulges with significantly smaller Sérsic index than a normal S0s sample closely matched in M_* and redshift. Both Xiao et al. (2016) and K. Xu et al. (2022) propose external gas accretion or minor mergers as the primary formation mechanism of SF S0s. Rathore et al. (2022) find that the SF S0s show a distinct size-mass relation compared to spirals, which indicates fading of spirals is unlikely the formation mechanism of SF S0s. From the IllustrisTNG simulation, Deeley et al. (2021) suggest that 37% of S0s form through gas stripping and 57% form through mergers.

Long-slit spectral observations have revealed that the phenomenon of gas-star counter-rotation is ubiquitous ($\sim 20\%$) in a small sample size (< 70) of S0s (Bertola et al. 1992; Kuijken et al. 1996; Kannappan & Fabricant 2001). Katkov et al. (2015) use the long-slit spectral observation from the Southern African Large Telescope to analyze a sample of S0s in isolated environment, finding that $\sim 39\% (= 7/18)$ of them display a visible counter-rotation. Meanwhile, Davis et al. (2011) find out that

36 ± 5 percent of fast-rotating early-type galaxies in the ATLAS^{3D} display gas-star kinematic misalignment. However, there are very few statistical studies of gas-star misalign fraction in S0s based on the integral field unit (IFU) survey due to the limited sample size. Thanks to the large IFU sample ($\sim 10,000$) of MaNGA, we are able to study the gas-star kinematic misalignment fraction in S0s with different stellar population for the first time. The data analysis is displayed in Section 2. The comparison of the properties for misaligned S0s to other types of galaxies are in Section 3. We propose external misaligned gas acquisition as an efficient formation mechanism of S0 galaxies with global $D_n4000 < 1.6$ in Section 4 and present our conclusions in Section 5.

2. DATA ANALYSIS

2.1. *MaNGA Survey*

MaNGA is one of three programmes in the fourth-generation SDSS (SDSS-IV) which starts on July 2014 (Bundy et al. 2015; Drory et al. 2015; Yan et al. 2016; Blanton et al. 2017). The science goal of MaNGA is to better understand how galaxies evolve and what regulates the star-formation, and it provides the spatially resolved spectroscopy with an unprecedented sample of $\sim 10,000$ nearby galaxies at a spatial resolution of ~ 1 kpc at median redshift $z \sim 0.03$. The targets are divided into ‘primary’ and ‘secondary’ samples, where the radial coverage is out to ~ 1.5 effective (half-light) radius R_e for the primary sample and $\sim 2.5R_e$ for the secondary sample (Yan et al. 2016). The Data Reduction Pipeline (Law et al. 2016, DRP) offers sky-subtracted and flux-calibrated 3D spectra of each galaxy, while the Data Analysis Pipeline (Westfall et al. 2019, DAP) analyzes DRP-processed spectra to measure the stellar kinematics, nebular emission-line kinematics, and spectral indices such as D_n4000 .

The global stellar mass (M_*) are obtained from the NASA-Sloan Atlas¹ (NSA; Blanton et al. 2011) which is estimated from the spectral energy distribution (SED) fitting using the K -correction code. The global D_n4000 is obtained by stacking the spectra with a median spectral signal-to-noise ratio (S/N) per pixel greater than 2 across the entire MaNGA bundle.

2.2. *Photometric Parameters and Morphological Classification*

¹ <http://nsatlas.org/>

The MaNGA PyMorph catalogue provides photometric parameters² and morphological classification³ (Domínguez Sánchez et al. 2022). The PyMorph photometric catalogue has single Sérsic fitting for Sérsic index and two components Sérsic+Exponential fitting for bulge-to-total light ratio (B/T), bulge effective radius R_e and bulge apparent magnitude. We use the r -band photometric parameters in this work and convert the r -band apparent magnitude m_r to absolute magnitude M_r based on the NSA redshift. Using the deep learning method, PyMorph morphological catalogue provides the numerical Hubble stage T-Type (de Vaucouleurs 1977, $T < 0$ corresponding to early-type galaxies), probabilities for being late-type galaxies (P_{LTG}) and S0s (P_{S0}) based on the analysis of SDSS DR7 image data. This catalogue also provides visual inspection results as visual class (VC=2 for S0s) and visual flag (VF=0 for reliable visual class). By cross-matching MPL-10 galaxies with the PyMorph catalogue, we obtain 9247 galaxies in total. We adopt the same selection criterion outlined in Domínguez Sánchez et al. (2022) to select S0s: $P_{LTG} < 0.5$, T -Type < 0 , $P_{S0} > 0.5$, $VC = 2$ and $VF = 0$. This criterion generates a sample of 789 S0s. We then check the images from the Dark Energy Spectroscopic Instrument (Dey et al. 2019, DESI) survey to remove cases of on-going mergers, leading to a final sample of 753 S0s. We apply the same criteria as in Domínguez Sánchez et al. (2022) to select 4534 spirals ($P_{LTG} > 0.5$, T -Type > 0 , $VC = 3$ and $VF = 0$) and 2117 ellipticals ($P_{LTG} < 0.5$, T -Type < 0 , $P_{S0} < 0.5$, $VC = 1$ and $VF = 0$). 1843 galaxies which do not satisfy the above criteria are classified as others including irregulars or spiral galaxies viewing edge-on.

2.3. Galaxies with Kinematic Misalignment

In order to obtain robust measurements on gas kinematics, we select emission-line galaxies as those with the $\text{H}\alpha$ emission-line S/N greater than 3 for at least 10 percent spaxels within $\sim 1.5R_e$. Out of 9247 MPL-10 galaxies in the PyMorph catalogue, 6938 emission-line galaxies are selected. To quantify the kinematic misalignment between gas and stars, the position angle (PA) of kinematic major axis is determined using PaFit package in Python (Krajnović et al. 2006). Misaligned galaxies are then defined as $\Delta PA \equiv |PA_{\text{gas}} - PA_{\text{star}}| > 30^\circ$,

where PA_{gas} and PA_{star} are PA for gaseous and stellar components, respectively. We select 723 candidates of misaligned galaxies with robust PA measurements $PA_{\text{error}} \leq 20^\circ$, where PA_{error} represents $\pm 1\sigma$ error of PAs. 456 of them are visually verified as our final sample of misaligned galaxies, where ongoing mergers or galaxies with irregular morphology are removed. For more details about the selection of misaligned galaxies, we refer readers to Zhou et al. (2022).

Fig. 1 presents an example of misaligned S0 galaxy while panel (a) shows the SDSS false-color image and the purple hexagon marks the MaNGA bundle. Panels (b) and (c) show the stellar and gaseous velocity fields, respectively. The red side moves away from us while the blue side approaches us. The rotation or angular momentum direction of the gas and stars are clearly opposite. For each component, PA is marked by the black solid line while the two blue dashed lines indicate its $\pm 1\sigma$ errors.

2.4. Merger Remnant Features

Based on DESI survey, we search for faint merger remnant features of the 9247 MPL-10 galaxies in the PyMorph catalogue. The DESI images are ~ 2 mag deeper than SDSS in the g -, r -band. The DESI surveys cover $\sim 14000 \text{ deg}^2$ of sky and are composed of three public projects. These include the Beijing-Arizona Sky Survey (BASS; Zou et al. 2017), which provides g -band and r -band images on the Bok 2.3-m telescope; the Mayall z -band Legacy Surveys (MzLS; Silva et al. 2016), which provides z -band images on the 4-m Mayall telescope; the Dark Energy Camera Legacy Survey (DECaLS; Blum et al. 2016), which provides g -band, r -band and z -band images on the 4-m Blanco telescope. Following the procedure described in Li et al. (2021), we convolve the r -band image with a Gaussian kernel to match the resolution of the g -band image and stack them together to increase the S/N. Based on the stacked images, we divide galaxies into isolated and interacting ones. Fig. 2 shows examples of galaxies with interacting features, including: (a) on-going mergers; (b) galaxies with tidal features; (c) galaxies with extended asymmetric stellar halos; (d) galaxies with shells. Our analysis identifies 737 galaxies with merger remnant features (b, c, d).

2.5. Sample and Control Sample Selection

In this work, we focus on S0 galaxies and split them into three subgroups for comparison: (a) S0s with kinematic misalignment, which is the S0 sample in Section 2.2 crossmatch with the misaligned galaxy sample in Section 2.3; (b) S0s with merger remnant features, which is the S0 sample crossmatch with the merger

² PyMorph photometric Value Added Catalogue: https://www.sdss4.org/dr17/data_access/value-added-catalogs/?vac_id=manga-pymorph-dr17-photometric-catalog

³ MaNGA Deep Learning Morphological Value Added Catalogue: https://www.sdss4.org/dr17/data_access/value-added-catalogs/?vac_id=manga-morphology-deep-learning-dr17-catalog

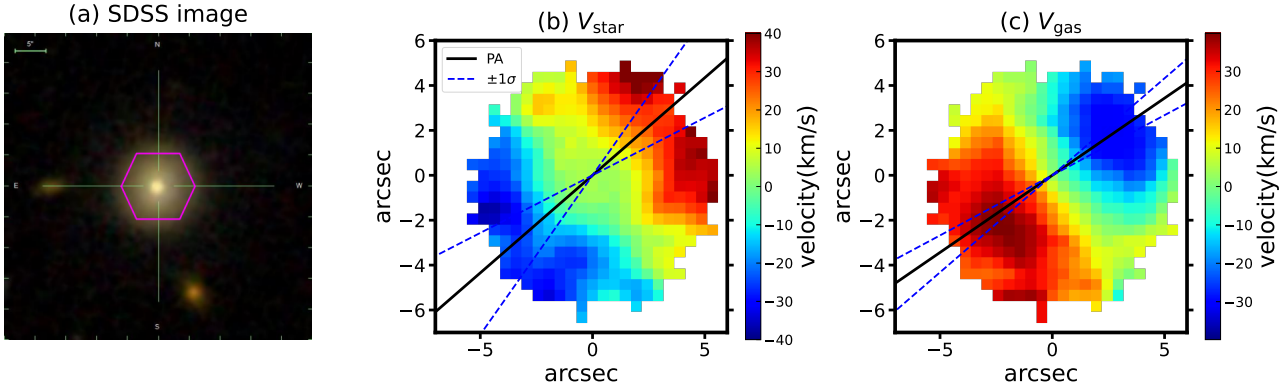


Figure 1. An example of misaligned S0 galaxy. Panel (a) displays the SDSS g , r , i -band false-color images with the purple hexagon marking the MaNGA bundle. Panel (b) and (c) show the velocity fields for the stellar and gaseous (traced by H α) components, respectively. The red side moves away from us while the blue side moves towards us. The black solid lines mark the position angle of kinematic major axes with two blue dashed lines being their $\pm 1\sigma$ errors.

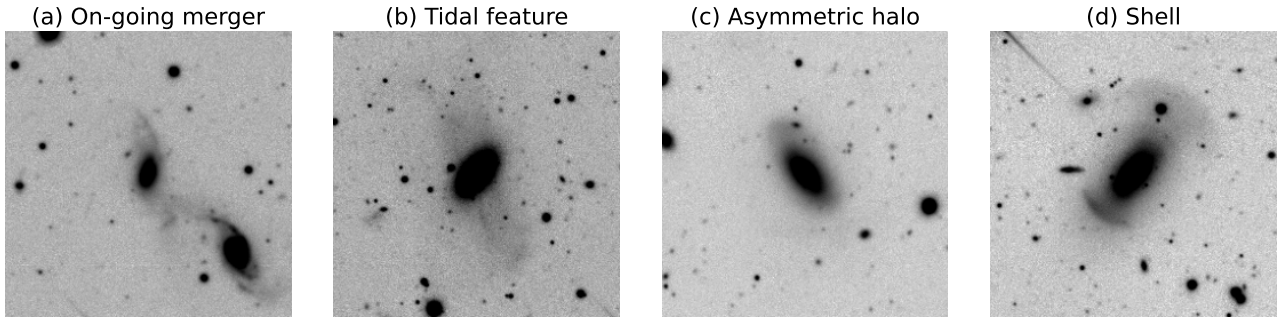


Figure 2. Classification of galaxies with interacting features: (a) on-going merger; (b) a galaxy with tidal features; (c) a galaxy with extended asymmetric stellar halo; (d) a galaxy with shell.

Table 1. Classification of MPL-10 galaxies crossmatch with PyMorph catalogue in different morphological types

Type	total	spiral	S0	elliptical	other
MPL-10 galaxies in PyMorph	9247	4534	753	2117	1843
Emission-line galaxies	6938	4393	429	758	1358
Misaligned galaxies ^(a)	456	56	89	176	135
Galaxies with merger remnant features ^(b)	737	239	67	285	146

remnant sample in Section 2.4; (c) aligned S0s which are emission-line galaxies without kinematic misalignment. We check the potential overlap between galaxies in (a) and (b), finding that only 7 out of 753 S0s exhibit both misalignment and merger remnant features. Since merger can also cause kinematic misalignment, we put them into subgroup (b). The classification of MPL-10 galaxies with different morphology is listed in the Table 1.

In order to compare S0s with other morphological types, we build a non-S0 control sample with the minimal distance to the S0s in $\log M_*$ versus global D_n4000 space, which is defined as $d = \sqrt{(\Delta \log M_*/0.1)^2 + (\Delta D_n4000/0.05)^2}$. $\Delta \log M_*$ and

ΔD_n4000 are the difference in $\log M_*$ and D_n4000 between a S0 galaxy and its control galaxy, respectively. We choose the global D_n4000 instead of star-formation rate (SFR) to select the control sample because this parameter has a consistent measurement for all types of galaxies and avoids potential effect over the emission-line strength due to interactions between accreted and pre-existing gas in misaligned galaxies. Since the global D_n4000 can reflect the age of galaxy stellar population, we split galaxies into young population with global $D_n4000 < 1.6$ (young galaxies for short), as well as old population with global $D_n4000 > 1.6$ (old galaxies).

Fig. 3 displays the global D_n4000 versus $\log(M_*/M_\odot)$ diagram for S0 galaxies (red squares) and their non-S0

control sample (blue open squares), with grey circles being MPL-10 galaxies. The horizontal dashed line corresponds to $D_n4000 = 1.6$ which roughly splits galaxies into young and old population. The top and right panels show the distribution of stellar masses and global D_n4000 for the S0s (red) and their controls (blue) respectively, with each distribution normalized to their sample size.

3. RESULTS

3.1. Misalign and Merger Remnant Fraction

We present a comparison of the gas-star misalign fraction (Fig. 4a & 4b) and merger remnant fraction (Fig. 4c) in galaxies which have different morphological types, including spirals (blue circles), S0s (green squares) and ellipticals (red triangles). To compare galaxies with different stellar population, we split galaxies into young and old population. We also include the non-S0 control sample built in Section 2.5 (grey triangles) in this comparison. In Fig. 4a, we show the misalign fraction which is defined as $N_{\text{mis}}/N_{\text{all}}$, where N_{mis} is the number of misaligned galaxies and N_{all} is the total number of galaxies (including galaxies with and without emission-lines) within a certain morphological type and stellar population bin. Since the kinematic misalignment can only be measured for emission-line galaxies due to the requirement of robust gas kinematics, we also present the comparison of misalign fraction $N_{\text{mis}}/N_{\text{eml}}$ in Fig. 4b, where N_{eml} is the number of emission-line galaxies within a certain morphological type and stellar population bin. The emission-line galaxies sample is only used in this section for comparison of misalign fraction and samples in other sections all contain lineless galaxies.

Fig. 4a shows that the fraction of S0s in general (young+old) population is $\sim 11\%$, which is the highest compared to spirals ($\sim 1\%$), ellipticals ($\sim 6\%$) as well as the control sample ($\sim 8\%$). Once we split the galaxies into young and old population, the differences between misalign fraction in S0s and other morphological types become more obvious for the young population ($\sim 15\%$ for the misaligned S0s), and less obvious for the old population ($\sim 10\%$ for the misaligned S0s). In Fig. 4b, the misalign fraction in emission-line S0s among the general (young+old) population is $\sim 19\%$. This fraction is consistent with previous work using a small sample (< 70) of S0s ($\sim 20\%$, Bertola et al. 1992; Kuijken et al. 1996; Kannappan & Fabricant 2001) where kinematic misalignment is defined within emission-line galaxies. The misalign fraction is much higher in Fig. 4b than Fig. 4a for S0s and ellipticals with old stellar population. This is because nearly half of early-type galaxies (ETGs) are

lineless. In summary, both Fig. 4a and Fig. 4b show that the young S0s have the highest misalign fraction, indicating a possible connection between kinematic misalignment and the formation of young S0s.

In Fig. 4c, we present merger remnant fraction in galaxies with different morphological types and stellar population. The merger remnant fraction in S0s is $\sim 9\%$ for the general population (young+old), lower than the $\sim 13\%$ for ellipticals, similar to that of spirals and non-S0 control sample. These trends are similar if we split the sample into young and old population. The difference of the merger remnant fraction in S0s and ellipticals becomes more obvious for young population. Comparing Fig. 4c & 4a, the misalign fraction in S0s is comparable to merger remnant fraction in S0s for the general population ($\sim 11\%$ vs. $\sim 9\%$), and this is also true for young population ($\sim 15\%$ vs. $\sim 13\%$) and old population ($\sim 10\%$ vs. $\sim 8\%$). Considering that kinematic misalignment phenomenon is believed to be primarily contributed by external gas acquisition, this result may indicate that external gas acquisition in S0s is as equally efficient as mergers. We will discuss misaligned gas acquisition as a formation mechanism of S0s in Section 4.

3.2. Photometric Properties

To explore the impact of external gas acquisition on galaxy morphology, we compare the photometric properties of galaxies with different morphological types. Fig. 5a shows B/T vs. Sérsic index n distribution, grey dots represent the entire S0 sample, while the blue contours represent the spirals and red contours represent the ellipticals. The green triangles and blue stars are misaligned S0s and misaligned spirals, respectively. As we expect, misaligned S0s locate in between spirals and ellipticals, while they have significant higher Sérsic index than misaligned spirals. We also find that misaligned spirals have higher B/T and Sérsic index than the entire spiral sample, which indicates misaligned gas acquisition can lead to bulge growth.

Fig. 5b presents the r -band bulge absolute magnitude M_r vs. bulge effective radius R_e . Grey dots represent the entire S0 sample, while green triangles, magenta squares and blue stars are misaligned S0s, merger remnant S0s and misaligned spirals, respectively. The aligned S0s are displayed as grey solid contours, while the entire spiral and elliptical samples are shown as blue dashed and red dashed contours, respectively. The misaligned S0s, aligned S0s and merger remnant S0s form a continuous sequence in bulge M_r vs. R_e diagram. Misaligned S0s dominate at lower bulge luminosity end with $\sim 1.5\text{mag}$ fainter compared to higher luminosity end in merger remnant S0s and they display significantly

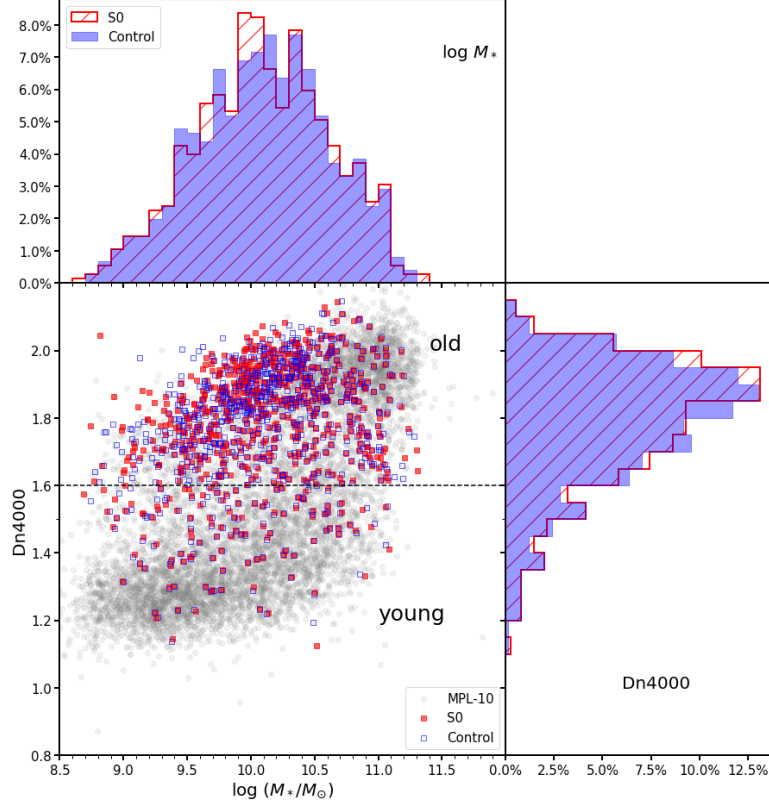


Figure 3. Global D_n 4000 versus $\log(M_*/M_\odot)$ diagram for S0 galaxies and their non-S0 control sample, with the grey circles being MPL-10 galaxies. Red squares represent S0 galaxies and blue open squares are their corresponding controls. The horizontal lines correspond to D_n 4000 = 1.6 which split galaxies into young and old population. The top and right panels show distribution of stellar masses and global D_n 4000 for the S0 galaxies (red) and their control samples (blue) respectively, with each distribution is normalized with respect to their sample size.

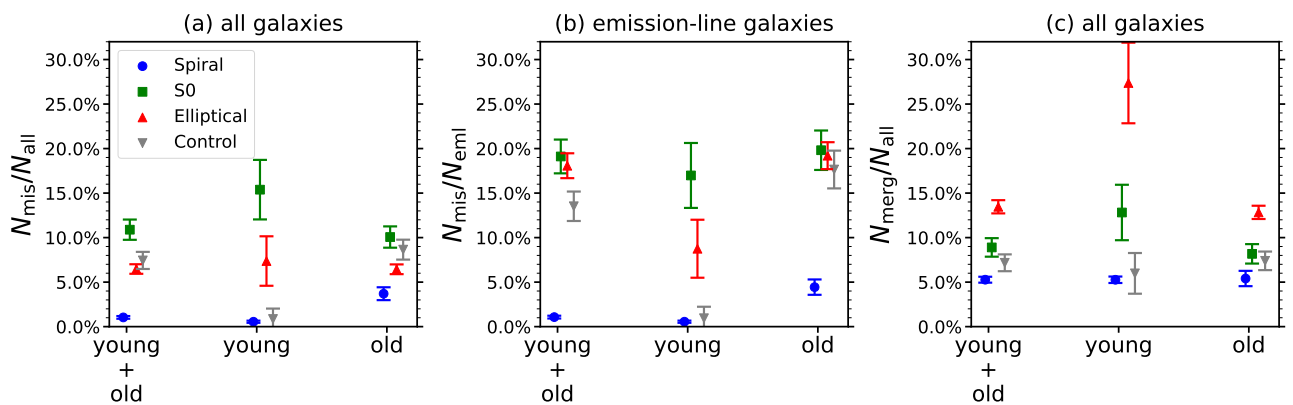


Figure 4. Panel (a) and (c) show the misalign fraction and merger remnant fraction in the entire MaNGA sample, respectively. Panel (b) shows the misalign fraction in the emission-line galaxies sample. Blue circles are for spiral galaxies, green squares for S0 galaxies and red triangles for elliptical galaxies. Each morphological type is divided into young and old population. Grey triangles represent the non-S0 control samples closely matched in M_* and global D_n 4000 for S0 galaxies. Each point in the same population (young, old and young+old) is slightly offset in the x -axis to avoid overlap.

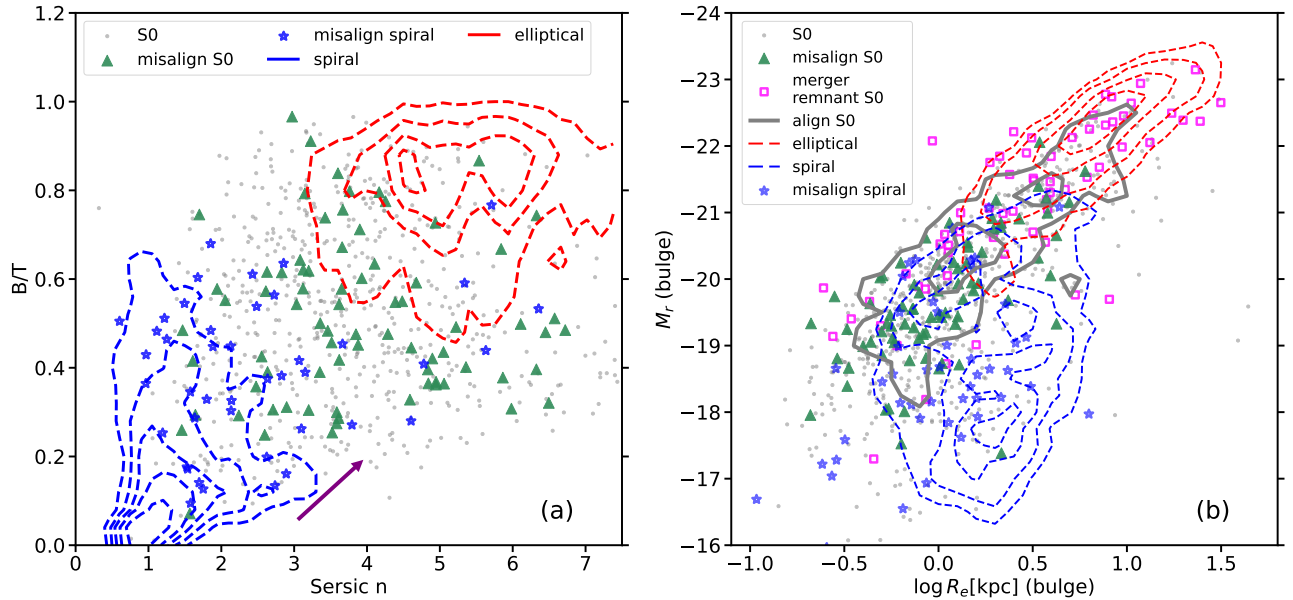


Figure 5. The panel (a) shows B/T vs. Sérsic index n distribution. Grey dots represent the entire S0 sample, while the blue contours represent the spirals and red contours represent the ellipticals. The green triangles and blue stars are misaligned S0s and misaligned spirals, respectively. The purple arrow indicates the direction of a continuous distribution for misaligned spirals and misaligned S0s. The panel (b) shows the r -band bulge absolute magnitude M_r vs. bulge effective radius R_e . Grey dots represent the entire S0 sample, while green triangles, magenta squares and blue stars are misaligned S0s, merger remnant S0s and misaligned spirals, respectively. The aligned S0s are displayed as grey solid contours while spiral galaxies and elliptical galaxies are shown as blue dashed and red dashed contours, respectively.

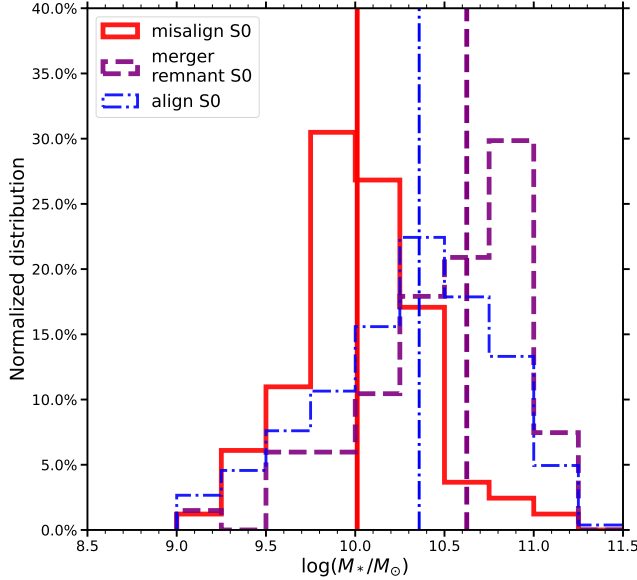


Figure 6. The distribution of stellar mass M_* for misaligned S0s (red solid), aligned S0s (blue dashed-dotted) and merger remnant S0s (purple dashed). Each distribution is normalized to their sample size. The vertical lines with the same color as histograms are the median of the distributions.

smaller bulge size, indicating misaligned S0s have different formation mechanism as merger. The aligned S0s have a wide coverage in bulge M_r vs. R_e diagram which are partially overlapped with both misaligned S0s and merger remnant S0s. Misaligned S0s have similar range of bulge R_e as spirals and misaligned spirals, but at a certain radius they have highest bulge luminosity compared to lower value in misaligned spirals and the lowest value in the entire spiral sample, indicating the connection between kinematic misalignment and growth of bulge.

3.3. Stellar and Dark Matter Halo Mass Distributions

We show the distribution of stellar mass M_* in Fig. 6 for misaligned S0s (red solid), aligned S0s (blue dashed-dotted) and merger remnant S0s (purple dashed). The vertical lines with the same color as the histograms represent the median of each distribution. Misaligned S0s have lower M_* (median value of $\sim 10^{10.0} M_\odot$) than merger remnant S0s (median value of $\sim 10^{10.6} M_\odot$), while aligned S0s have widest M_* distribution with a median value of $\sim 10^{10.4} M_\odot$.

We then compare the environmental properties by using group halo mass and the number of group members taken from Yang et al. (2007). They develop a method to categorize member galaxies into a galaxy group. Unlike the traditional friend-of-friend method, this technique can identify groups with only one member galaxy.

They measure the group characteristic luminosity $L_{19.5}$, defined as the total luminosity of all group members down to $M_r - 5 \log h \leq -19.5$ ($h = 0.73$) with completeness correction. To obtain the halo mass of a given group, they first assume a one-to-one relation between the $L_{19.5}$ to halo masses. When a group halo mass function is given in a comoving volume, galaxy groups can be assigned halo masses according to their rank orders of $L_{19.5}$ (the highest halo mass is assigned to the galaxy group with the highest $L_{19.5}$). We present the distribution of group halo mass M_{halo} and the number of group members for each galaxy of its galaxy group in Fig. 7a & 7b, respectively. The misaligned S0s (red) tend to reside in lower mass host group halos (median value of $M_{\text{halo}} \sim 10^{12} M_\odot$) and the merger remnant S0s (purple) tend to reside in higher mass host group halos (median value of $M_{\text{halo}} \sim 10^{12.9} M_\odot$), while the aligned S0s (blue) cover a wider range of halo mass with a median value of $\sim 10^{12.7} M_\odot$. In Fig. 7b, misaligned S0s show the smallest number of member galaxies compared to merger remnant S0s and aligned S0s. Our results are consistent with Davis et al. (2011), who discover that galaxies in dense groups and Virgo cluster always have aligned kinematics while $42 \pm 5\%$ of fast-rotating ETGs have kinematic misalignment. Also, Lagos et al. (2014) use the galaxy formation model GALFORM to show that gas-rich early-type galaxies tend to locate in low-mass halos.

3.4. Stellar Population

Fig. 8 presents the radial gradient of $D_{n,4000}$ for S0s with different types. Thick lines represent the median of $D_{n,4000}$ in each R/R_e bin while shaded regions with the same color give the $\pm 1\sigma$ error of $D_{n,4000}$ measurement. Red dashed lines with hollowed squares are misaligned S0s, cyan dashed-dotted lines are aligned S0s while purple dotted lines with filled dots are merger remnant S0s. The left and right panel show galaxies with young and old stellar population, respectively.

Fig. 8a shows the young misaligned S0s have positive $D_{n,4000}$ radial gradient, which indicates younger stellar population in the central region compared to their outskirts. The aligned S0s and merger remnant S0s show negative $D_{n,4000}$ radial gradient. The lower $D_{n,4000}$ for merger remnant S0s than aligned S0s could be due to merger induced star-formation. In Fig. 8b, the old misaligned S0s, aligned S0s and S0s with merger remnant features display very similar $D_{n,4000}$ radial profile with a clear negative radial gradient.

4. DISCUSSION

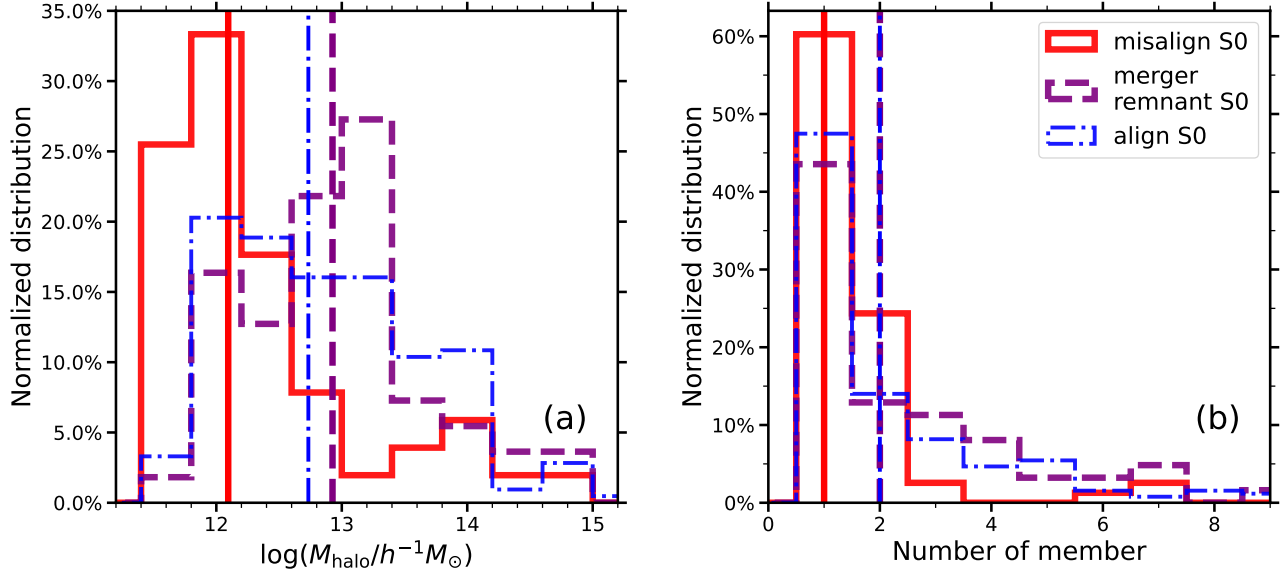


Figure 7. Panel (a) and (b) show the distribution of group halo mass M_{halo} and number of group members for galaxies within their galaxy group, respectively. Misaligned S0s, aligned S0s and merger remnant S0s are represented by red solid, blue dashed-dotted and purple dashed histograms, respectively. Each distribution is normalized to their sample size. The vertical lines with the same color as histograms are the median of the distributions.

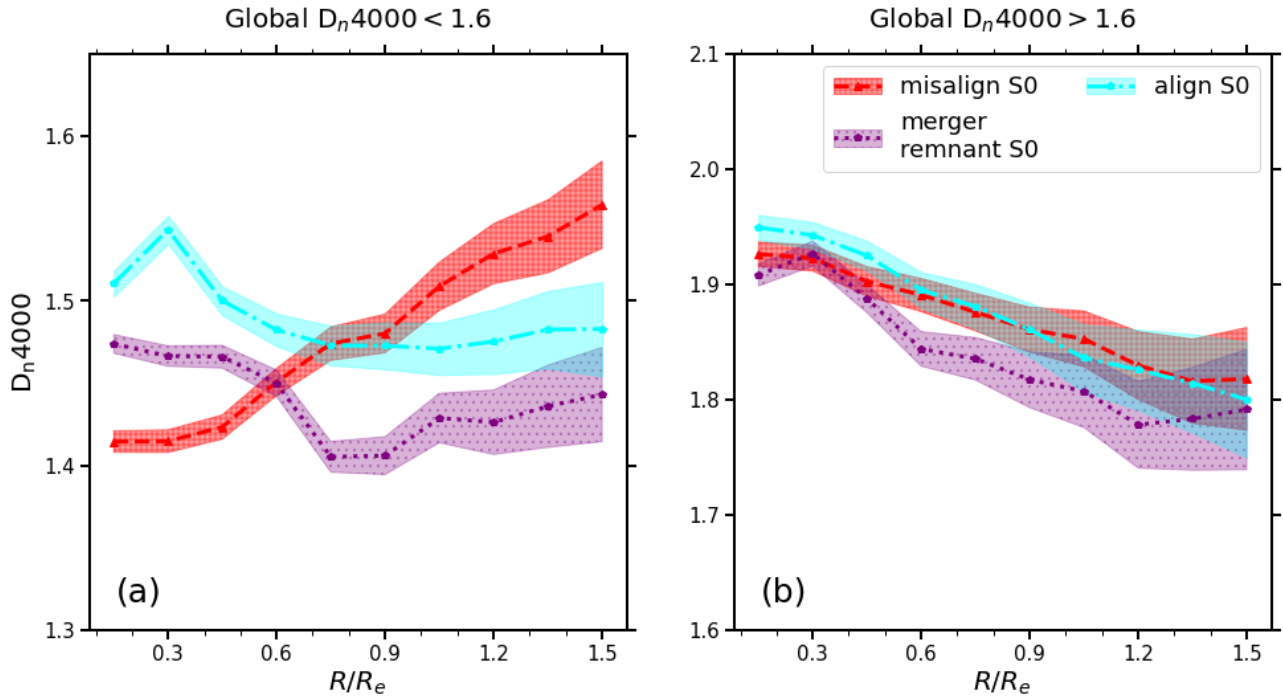


Figure 8. The D_n4000 radial gradients for young (left) and old (right) misaligned S0s (red dashed), aligned S0s (cyan dashed-dotted) and merger remnant S0s (purple dotted). Thick lines represent the median of D_n4000 in each R/R_e bin while shaded regions with same color are the $\pm 1\sigma$ error of D_n4000 measurement.

In Section 3.1, we show that misalign fraction in S0s is the highest among all the morphological types. Therefore, this leads to the question whether there is any connection between kinematic misalign phenomena and the formation of S0s?

Based on the IllustrisTNG simulation, [Deeley et al. \(2020\)](#) point out merger and gas stripping in dense environment (faded spiral) are two dominated mechanisms in the formation of S0s. However, neither of these two mechanisms can explain the properties of misaligned S0s. On the one hand, misaligned S0s have significantly lower bulge luminosity and smaller bulge size compared to merger remnant S0s or ellipticals (see Fig. 5), indicating major merger is not the dominated formation mechanism of misaligned S0s. On the other hand, comparing with aligned S0s and merger remnant S0s, misaligned S0s tend to locate in isolated environment (Fig. 7), indicating gas stripping which tends to happen in dense environment is not the dominated formation mechanism of misaligned S0s. Meanwhile the positive D_{n4000} radial gradient of misaligned S0s (Fig. 8) is not able to be explained by faded spiral if gas is stripped at outskirts.

Putting all these observational results together with the truth that S0s have the highest misalign fraction among all the galaxy morphology type, we propose misaligned gas acquisition scenario for the formation of misaligned S0s, especially in young galaxies. The accreted gas interacts with pre-existing gas leading to angular momentum redistribution which triggers gas inflow and the central star-formation ([Jin et al. 2016](#); [Chen et al. 2016](#); [H. Xu et al. 2022](#); [Zhou et al. 2022](#)).

4.1. Bulge Growth from Misaligned Gas Acquisition

To explore the influence of external gas acquisition on bulges growth, we compare the B/T (panel a) and λ_{R_e} (panel b) in Fig. 9 for misaligned S0s (red solid), aligned S0s (blue dashed-dotted), misaligned spirals (cyan shaded) and aligned spirals (grey shaded). The vertical lines with the same color as the histograms are the median of the distributions. The spin parameter λ_{R_e} is a proxy of the specific angular momentum for stars defined as

$$\lambda_{R_e} = \frac{\sum_{i=1}^{N_p} F_i R_i |V_i|}{\sum_{i=1}^{N_p} F_i R_i \sqrt{V_i^2 + \sigma_i^2}}, \quad (1)$$

where F_i , V_i , σ_i are the r -band flux, stellar velocity and stellar velocity dispersion of the i -th spaxel within R_e . R_i is the distance between the i -th spaxel and the galaxy center. Larger λ_{R_e} means higher specific angular momentum ([Emsellem et al. 2007](#)). Fig. 9a shows that the misaligned spirals have similar B/T as S0s (misaligned and aligned), which is much higher than aligned spirals.

Fig. 9b shows that both misaligned S0s and misaligned spirals have much lower λ_{R_e} than aligned spirals, while their λ_{R_e} is similar or even lower than aligned S0s. One natural explanation to the higher B/T and lower λ_{R_e} in misaligned S0s and misaligned spirals in Fig. 9 is misaligned gas acquisition, where the accreted gas interacts with pre-existing gas leading to gas inflow and the growth of bulge component.

4.2. Lower Spiral Arm Fraction in Misaligned Galaxies

The formation of S0s includes growth of bulge and fading of spiral arm features. In Section 4.1, we show the impact of misaligned gas acquisition on the growth of bulge. In this section, we explore the impact of misaligned gas acquisition on the spiral arm fading. Since PyMorph catalogue does not classify disk galaxies from spirals, we visually check the SDSS image to separate disk galaxies from spirals. For misaligned spirals, we build an control sample which is aligned spirals with similar M_* , global D_{n4000} , inclination angle and redshift. Fig. 10 shows the fraction of galaxies with spiral arm features in misaligned and aligned control samples. Red histograms with hatched lines are misaligned galaxies while the cyan histograms are aligned controls. For both young and old samples, the fraction of galaxies with spiral arm features is much lower in misaligned galaxies than that in aligned controls. It is intriguing that none of the young misaligned spirals (classified as spirals by PyMorph) shows spiral arm features. This suggests misaligned gas acquisition contributes to the formation of disk galaxies, where quenching happens at the outskirts of galaxies indicated by the positive D_{n4000} gradient of misaligned S0s in Fig. 8a.

Simulation works also shed light on the relation between spiral arms fading and gas-star counter-rotation. Based on the N -body simulations GADGET-3, [D’Onghia et al. \(2013\)](#) compare two galaxies with only difference in the rotational direction of gaseous components, finding that the spiral arms cannot form once the gaseous components are counter-rotating. [Osman & Bekki \(2017\)](#) obtain similar results through smoothed-particle hydrodynamical simulation, suggesting that the existence of counter-rotating gas suppress the swing amplification mechanism for the formation of spiral arms ([Toomre 1981](#); [Michikoshi & Kokubo 2016](#)). These simulations are qualitatively consistent with our results.

Combining observational results in Section 4.1 & 4.2, we suggest misaligned gas acquisition have significant impact over galaxy morphology with growth of bulge and fading of spiral arms, which leads to formation of S0s.

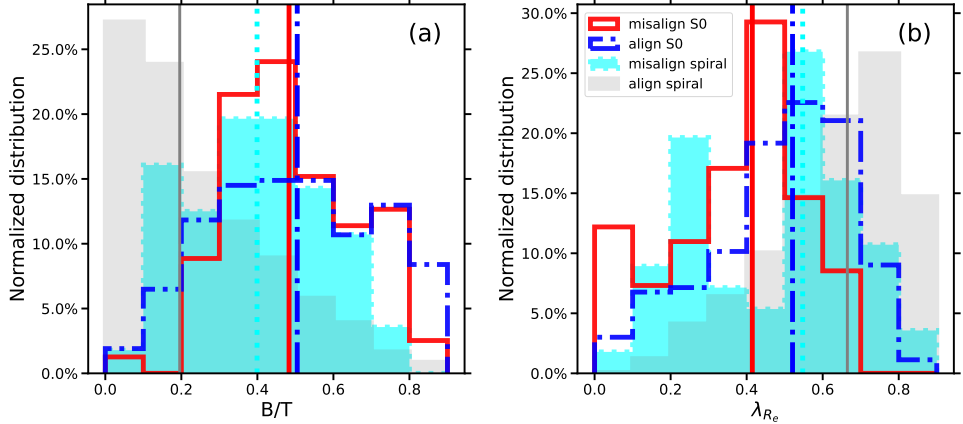


Figure 9. Panel (a) shows B/T distribution and panel (b) shows the λ_{R_e} distribution. Misaligned S0s, aligned S0s, misaligned spirals and aligned spirals are represented by red solid, blue dashed-dotted, cyan shaded and grey shaded, respectively. Each distribution is normalized to their sample size. The vertical lines with the same color as histograms are the median of the distributions.

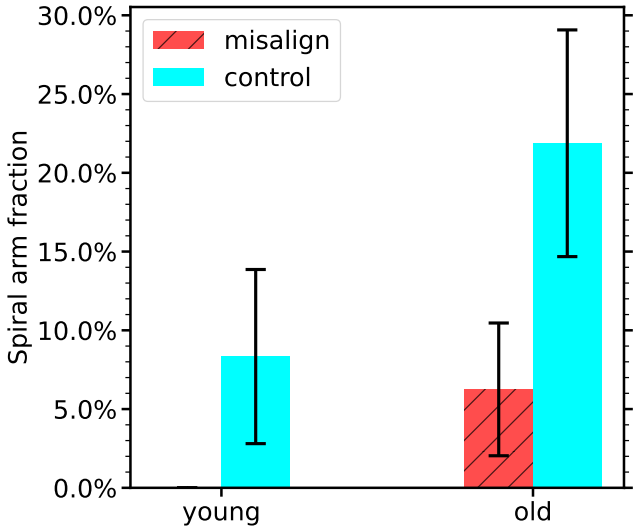


Figure 10. Fraction of galaxies with spiral arm features in misaligned and aligned control galaxies with different stellar population. Red histograms with hatched lines are misaligned galaxies while the cyan histograms are aligned controls.

4.3. The Contribution of Mergers in Misaligned Galaxies

The visibility timescale of merger remnant features depends on both the observation depth and the time at which merging process happened. Using N-body hydrodynamic simulations GADGET2, Ji et al. (2014) find that the visibility timescale of merger remnant features is $\gtrsim 1.4$ Gyr for r -band surface brightness limit $\mu_r = 25$ mag arcsec^{-2} , while the timescale is $\gtrsim 5$ Gyr for $\mu_r = 28$ mag arcsec^{-2} . We observe 66 misaligned galaxies with APO-3.5m telescope in the white-light mode, where the surface brightness limit is ~ 28 mag arcsec^{-2} ,

finding that $< 5\%$ of these misaligned galaxies show merger remnant features. The surface brightness limit for the DESI survey, which is used for our merger remnant classification, is ~ 27 mag arcsec^{-2} . Therefore, combining this result with significant differences between bulge luminosity and radius between misaligned S0s and merger remnant S0s (see Fig. 5b), we conclude mergers are not the main driver in the formation of misaligned S0s.

Observational and simulation studies also reveal that although mergers give rise to kinematic misalignment, it is not a dominated mechanism. From observational studies, Li et al. (2021) find that the merger remnant fraction are similar between SF misaligned galaxies and aligned galaxies, indicating mergers are not the primary origin of misalignment in SF galaxies. Meanwhile the merger remnant fraction in quiescent (QS) misaligned galaxies is $\sim 10\%$ higher than the merger remnant fraction in aligned galaxies, indicating mergers have contribution to misalignment in QS galaxies, but not the dominated mechanism. From simulation studies, Lagos et al. (2015) use the GALFORM model of galaxy formation to investigate misalign fraction in ETGs, finding that the misalign fraction is 2–5% with only merger process, when they add gas accretion, this fraction increases to $\sim 46\%$ which is consistent with ATLAS^{3D} observational result ($\sim 42\%$ for ETGs). Based on the Illustris simulations, Starkenburg et al. (2019) find that mergers alone cannot account for the misaligned fraction in low-mass galaxies with $\log(M_*/M_\odot) < 10.7$. Therefore, we prefer gas accretion as the primary mechanism for the formation of misaligned galaxies.

5. CONCLUSIONS

We analyze a sample of 753 S0 galaxies from the MPL-10 of MaNGA survey and investigate the gas-star kinematic misalignment fraction and merger remnant fraction in galaxies with different morphological types. We compare the r -band photometric parameters, stellar mass, group halo mass and number of group members as well as stellar population between misaligned S0s and other types of galaxies. The results are the following:

(i) the misalign fraction in S0s is the highest among all the morphological types for both young and old galaxies, and it is comparable to merger remnant fraction in S0s;

(ii) in the bulge M_r vs. R_e diagram, misaligned S0s dominate at lower bulge luminosity end with significantly smaller bulge size compared to higher luminosity end in merger remnant S0s. The aligned S0s have a wide coverage in M_r vs. R_e diagram which are partially overlapped with both misaligned S0s and merger remnant S0s.

(iii) misaligned S0s have lower M_* (median value of $\sim 10^{10.0} M_\odot$) than merger remnant S0s (median value of $\sim 10^{10.6} M_\odot$), while aligned S0s have widest M_* distribution with a median value of $\sim 10^{10.4} M_\odot$;

(iv) misaligned S0s tend to reside in lower mass host group halos with lower number of member galaxies and merger remnant S0s tend to reside in higher mass host group halos with higher number of member galaxies, while the aligned S0s cover a wider range of halo mass and number of member galaxies;

(v) the young misaligned S0s have positive D_{n4000} radial gradients, indicating younger stellar population in the central region than the outskirts;

(vi) misaligned spirals have similar B/T as S0s (misaligned and aligned), which is much higher than aligned spirals, meanwhile both misaligned S0s and misaligned spirals have much lower λ_{R_e} than aligned spirals and their λ_{R_e} is similar or even lower than aligned S0s.

(vii) misaligned galaxies have lower fraction of spiral arm features than that of aligned galaxies;

Since misaligned S0s have distinct features compared to merger remnant S0s in bulge M_r vs. R_e diagram, M_* distribution as well as group environment properties, we conclude misaligned S0s have different formation mechanism as merger remnant S0s. Meanwhile, misaligned S0s locate in isolated environment, faded spiral is not the dominated formation mechanism of misaligned S0s. We propose misaligned gas acquisition as an efficient formation pathway for young S0 galaxies. The accreted gas interacts with pre-existing gas in galaxies, leading to angular momentum redistribution and gas inflow, which triggers central star-formation and bulge growth (ii, v,

vi). Meanwhile, the lack of cold gas at the outskirts leads to fading of spiral arms (vii).

ACKNOWLEDGEMENTS

Y. C acknowledges support from the NSFC grant 12333002 and the China Manned Space Project (grant No. CMS-CSST-2021-A05) as well as the China Manned Space Project (the second-stage CSST science project: “Investigation of small-scale structures in galaxies and forecasting of observations”). J.W. acknowledges support by the NSFC grants U1831205, 12033004 and 12221003. DB is partly supported by RSCF grant 22-12-00080.

This work is partly based on observations obtained with the Apache Point Observatory 3.5-meter telescope, which is owned and operated by the Astrophysical Research Consortium.

Funding for the Sloan Digital Sky Survey IV has been provided by the Alfred P. Sloan Foundation, the U.S. Department of Energy Office of Science, and the Participating Institutions.

SDSS-IV acknowledges support and resources from the Center for High Performance Computing at the University of Utah. The SDSS website is www.sdss.org.

SDSS-IV is managed by the Astrophysical Research Consortium for the Participating Institutions of the SDSS Collaboration including the Brazilian Participation Group, the Carnegie Institution for Science, Carnegie Mellon University, Center for Astrophysics — Harvard & Smithsonian, the Chilean Participation Group, the French Participation Group, Instituto de Astrofísica de Canarias, The Johns Hopkins University, Kavli Institute for the Physics and Mathematics of the Universe (IPMU) / University of Tokyo, the Korean Participation Group, Lawrence Berkeley National Laboratory, Leibniz Institut für Astrophysik Potsdam (AIP), Max-Planck-Institut für Astronomie (MPIA Heidelberg), Max-Planck-Institut für Astrophysik (MPA Garching), Max-Planck-Institut für Extraterrestrische Physik (MPE), National Astronomical Observatories of China, New Mexico State University, New York University, University of Notre Dame, Observatório Nacional / MCTI, The Ohio State University, Pennsylvania State University, Shanghai Astronomical Observatory, United Kingdom Participation Group, Universidad Nacional Autónoma de México, University of Arizona, University of Colorado Boulder, University of Oxford, University of Portsmouth, University of Utah, University of Virginia, University of Washington, University of Wisconsin, Vanderbilt University, and Yale University.

REFERENCES

Bekki, K. 1998, ApJL, 502, L133, doi: [10.1086/311508](https://doi.org/10.1086/311508)

Bekki, K., & Couch, W. J. 2011, MNRAS, 415, 1783, doi: [10.1111/j.1365-2966.2011.18821.x](https://doi.org/10.1111/j.1365-2966.2011.18821.x)

Bertola, F., Buson, L. M., & Zeilinger, W. W. 1992, ApJL, 401, L79, doi: [10.1086/186675](https://doi.org/10.1086/186675)

Blanton, M. R., Kazin, E., Muna, D., Weaver, B. A., & Price-Whelan, A. 2011, AJ, 142, 31, doi: [10.1088/0004-6256/142/1/31](https://doi.org/10.1088/0004-6256/142/1/31)

Blanton, M. R., Bershady, M. A., Abolfathi, B., et al. 2017, AJ, 154, 28, doi: [10.3847/1538-3881/aa7567](https://doi.org/10.3847/1538-3881/aa7567)

Blum, R. D., Burleigh, K., Dey, A., et al. 2016, in American Astronomical Society Meeting Abstracts, Vol. 228, American Astronomical Society Meeting Abstracts #228, 317.01

Blumenthal, G. R., Faber, S. M., Primack, J. R., & Rees, M. J. 1984, Nature, 311, 517, doi: [10.1038/311517a0](https://doi.org/10.1038/311517a0)

Bundy, K., Bershady, M. A., Law, D. R., et al. 2015, ApJ, 798, 7, doi: [10.1088/0004-637X/798/1/7](https://doi.org/10.1088/0004-637X/798/1/7)

Burstein, D., Ho, L. C., Huchra, J. P., & Macri, L. M. 2005, ApJ, 621, 246, doi: [10.1086/427408](https://doi.org/10.1086/427408)

Chen, Y.-M., Shi, Y., Tremonti, C. A., et al. 2016, Nature Communications, 7, 13269, doi: [10.1038/ncomms13269](https://doi.org/10.1038/ncomms13269)

Davis, T. A., Alatalo, K., Sarzi, M., et al. 2011, MNRAS, 417, 882, doi: [10.1111/j.1365-2966.2011.19355.x](https://doi.org/10.1111/j.1365-2966.2011.19355.x)

de Vaucouleurs, G. 1977, in Evolution of Galaxies and Stellar Populations, ed. B. M. Tinsley & D. C. Larson, Richard B. Gehret, 43

Deeley, S., Drinkwater, M. J., Sweet, S. M., et al. 2021, MNRAS, 508, 895, doi: [10.1093/mnras/stab2007](https://doi.org/10.1093/mnras/stab2007)

—. 2020, MNRAS, 498, 2372, doi: [10.1093/mnras/staa2417](https://doi.org/10.1093/mnras/staa2417)

Dey, A., Schlegel, D. J., Lang, D., et al. 2019, AJ, 157, 168, doi: [10.3847/1538-3881/ab089d](https://doi.org/10.3847/1538-3881/ab089d)

H. Xu, Chen, Y., Shi, Y., et al. 2022, MNRAS, 511, 4685, doi: [10.1093/mnras/stac354](https://doi.org/10.1093/mnras/stac354)

K. Xu, Gu, Q., Lu, S., et al. 2022, MNRAS, 509, 1237, doi: [10.1093/mnras/stab3013](https://doi.org/10.1093/mnras/stab3013)

Domínguez Sánchez, H., Margalef, B., Bernardi, M., & Huertas-Company, M. 2022, MNRAS, 509, 4024, doi: [10.1093/mnras/stab3089](https://doi.org/10.1093/mnras/stab3089)

D'Onghia, E., Vogelsberger, M., & Hernquist, L. 2013, ApJ, 766, 34, doi: [10.1088/0004-637X/766/1/34](https://doi.org/10.1088/0004-637X/766/1/34)

Dressler, A. 1980, ApJ, 236, 351, doi: [10.1086/157753](https://doi.org/10.1086/157753)

Drory, N., MacDonald, N., Bershady, M. A., et al. 2015, AJ, 149, 77, doi: [10.1088/0004-6256/149/2/77](https://doi.org/10.1088/0004-6256/149/2/77)

Emsellem, E., Cappellari, M., Krajnović, D., et al. 2007, MNRAS, 379, 401, doi: [10.1111/j.1365-2966.2007.11752.x](https://doi.org/10.1111/j.1365-2966.2007.11752.x)

Gunn, J. E., & Gott, J. Richard, I. 1972, ApJ, 176, 1, doi: [10.1086/151605](https://doi.org/10.1086/151605)

Hubble, E. P. 1926, ApJ, 64, 321, doi: [10.1086/143018](https://doi.org/10.1086/143018)

Icke, V. 1985, A&A, 144, 115

Ji, I., Peirani, S., & Yi, S. K. 2014, A&A, 566, A97, doi: [10.1051/0004-6361/201423530](https://doi.org/10.1051/0004-6361/201423530)

Jin, Y., Chen, Y., Shi, Y., et al. 2016, MNRAS, 463, 913, doi: [10.1093/mnras/stw2055](https://doi.org/10.1093/mnras/stw2055)

Kannappan, S. J., & Fabricant, D. G. 2001, AJ, 121, 140, doi: [10.1086/318027](https://doi.org/10.1086/318027)

Katkov, I. Y., Kniazev, A. Y., & Sil'chenko, O. K. 2015, AJ, 150, 24, doi: [10.1088/0004-6256/150/1/24](https://doi.org/10.1088/0004-6256/150/1/24)

Khochfar, S., & Silk, J. 2006, MNRAS, 370, 902, doi: [10.1111/j.1365-2966.2006.10533.x](https://doi.org/10.1111/j.1365-2966.2006.10533.x)

Krajnović, D., Cappellari, M., de Zeeuw, P. T., & Copin, Y. 2006, MNRAS, 366, 787, doi: [10.1111/j.1365-2966.2005.09902.x](https://doi.org/10.1111/j.1365-2966.2005.09902.x)

Kuijken, K., Fisher, D., & Merrifield, M. R. 1996, MNRAS, 283, 543, doi: [10.1093/mnras/283.2.543](https://doi.org/10.1093/mnras/283.2.543)

Lagos, C. d. P., Davis, T. A., Lacey, C. G., et al. 2014, MNRAS, 443, 1002, doi: [10.1093/mnras/stu1209](https://doi.org/10.1093/mnras/stu1209)

Lagos, C. d. P., Padilla, N. D., Davis, T. A., et al. 2015, MNRAS, 448, 1271, doi: [10.1093/mnras/stu2763](https://doi.org/10.1093/mnras/stu2763)

Larson, R. B., Tinsley, B. M., & Caldwell, C. N. 1980, ApJ, 237, 692, doi: [10.1086/157917](https://doi.org/10.1086/157917)

Laurikainen, E., Salo, H., Buta, R., Knapen, J. H., & Comerón, S. 2010, MNRAS, 405, 1089, doi: [10.1111/j.1365-2966.2010.16521.x](https://doi.org/10.1111/j.1365-2966.2010.16521.x)

Law, D. R., Cherinka, B., Yan, R., et al. 2016, AJ, 152, 83, doi: [10.3847/0004-6256/152/4/83](https://doi.org/10.3847/0004-6256/152/4/83)

Li, S.-l., Shi, Y., Bizyaev, D., et al. 2021, MNRAS, 501, 14, doi: [10.1093/mnras/staa3618](https://doi.org/10.1093/mnras/staa3618)

Michikoshi, S., & Kokubo, E. 2016, ApJ, 823, 121, doi: [10.3847/0004-637X/823/2/121](https://doi.org/10.3847/0004-637X/823/2/121)

Mo, H. J., Mao, S., & White, S. D. M. 1998, MNRAS, 295, 319, doi: [10.1046/j.1365-8711.1998.01227.x](https://doi.org/10.1046/j.1365-8711.1998.01227.x)

Osman, O., & Bekki, K. 2017, MNRAS, 471, L87, doi: [10.1093/mnrasl/slx104](https://doi.org/10.1093/mnrasl/slx104)

Querejeta, M., Eliche-Moral, M. C., Tapia, T., et al. 2015, A&A, 573, A78, doi: [10.1051/0004-6361/201424303](https://doi.org/10.1051/0004-6361/201424303)

Quilis, V., Moore, B., & Bower, R. 2000, Science, 288, 1617, doi: [10.1126/science.288.5471.1617](https://doi.org/10.1126/science.288.5471.1617)

Rathore, H., Kumar, K., Mishra, P. K., Wadadekar, Y., & Bait, O. 2022, MNRAS, 513, 389, doi: [10.1093/mnras/stac871](https://doi.org/10.1093/mnras/stac871)

Silva, D. R., Blum, R. D., Allen, L., et al. 2016, in American Astronomical Society Meeting Abstracts, Vol. 228, American Astronomical Society Meeting Abstracts #228, 317.02

Starkenburg, T. K., Sales, L. V., Genel, S., et al. 2019, ApJ, 878, 143, doi: [10.3847/1538-4357/ab2128](https://doi.org/10.3847/1538-4357/ab2128)

Toomre, A. 1981, in *Structure and Evolution of Normal Galaxies*, ed. S. M. Fall & D. Lynden-Bell, 111–136

Westfall, K. B., Cappellari, M., Bershady, M. A., et al. 2019, AJ, 158, 231, doi: [10.3847/1538-3881/ab44a2](https://doi.org/10.3847/1538-3881/ab44a2)

Wilman, D. J., Oemler, A., Jr., Mulchaey, J. S., et al. 2009, ApJ, 692, 298, doi: [10.1088/0004-637X/692/1/298](https://doi.org/10.1088/0004-637X/692/1/298)

Xiao, M.-Y., Gu, Q.-S., Chen, Y.-M., & Zhou, L. 2016, ApJ, 831, 63, doi: [10.3847/0004-637X/831/1/63](https://doi.org/10.3847/0004-637X/831/1/63)

Yan, R., Bundy, K., Law, D. R., et al. 2016, AJ, 152, 197, doi: [10.3847/0004-6256/152/6/197](https://doi.org/10.3847/0004-6256/152/6/197)

Yang, X., Mo, H. J., van den Bosch, F. C., et al. 2007, ApJ, 671, 153, doi: [10.1086/522027](https://doi.org/10.1086/522027)

Zhou, Y., Chen, Y., Shi, Y., et al. 2022, MNRAS, 515, 5081, doi: [10.1093/mnras/stac2016](https://doi.org/10.1093/mnras/stac2016)

Zou, H., Zhou, X., Fan, X., et al. 2017, PASP, 129, 064101, doi: [10.1088/1538-3873/aa65ba](https://doi.org/10.1088/1538-3873/aa65ba)